JOURNAL OF GEOPHYSICAL RESEARCH, VOL. 98, NO. A7, PAGES 11,401–11,410, JULY 1, 1993

Whistlers and Plasmaspheric Hiss: Wave Directions and Three-Dimensional Propagation

A. B. DRAGANOV, U. S. INAN, V. S. SONWALKAR, AND T. F. BELL

STAR Laboratory, Department of Electrical Engineering, Stanford University, Stanford, California

Wave data from the DE 1 satellite showing simultaneously nonducted whistlers and hiss are analyzed to determine wave propagation directions. At $L = 3.8$ and a geographic latitude of $\lambda_g = 12°$S, the average wave normal directions of discrete whistlers are measured to be ~51° for $f = 4.5$ kHz and ~60° for $f = 3.5$ kHz, forming a small (<20°) angle with the magnetic meridional plane. Hiss wave normal angles are determined as ~70° and ~77° for $f = 3.5$ kHz and $f = 2.5$ kHz, respectively, with the wave vector being almost perpendicular to the meridional plane. While the measured wave normal angles of whistlers and hiss are consistent with generation of hiss by magnetospheric whistlers, existence of a significant azimuthal component indicates that further assessment of this connection must be based on three-dimensional ray tracing. A new approximate analytical formulation of three-dimensional propagation of whistler waves is developed and used to model the drift of magnetospherically reflected whistlers in azimuth. The results show that depending on initial parameters, the time of arrival of whistler rays at a fixed observation point can differ by 10 – 20 s, with signals from different magnetospherically reflected whistlers overlapping to evolve into a hiss like signal. The total azimuthal drift of whistler rays is found to not exceed ~30°, so that plasmaspheric hiss may be produced by nonducted whistlers at longitudes correlated with the location of thunderstorm activity.

1. INTRODUCTION

The nature and origin of magnetospheric hiss, in particular that which is omnipresent within the plasmasphere, remains an open question in spite of work that has spanned over two decades [*Storey et al.*, 1991, and references therein]. Recent experimental evidence indicates a causative connection between whistler waves from lightning discharges and ELF/VLF hiss [*Sonwalkar and Inan*, 1989]. In addition, theoretical models have suggested that multiple reflections of whistlers in the magnetosphere can evolve into hiss and that the observed levels of hiss may be sustained by wave energy injected into the medium by lightning discharges [*Draganov et al.*, 1992]. In this paper, we further investigate the connection between whistlers and hiss by means of (1) measurement of the average propagation directions of whistlers and hiss and (2) by consideration of the three dimensional propagation of whistlers including the azimuthal spread of raypaths so as to assess the size of magnetospheric regions that are likely to be excited by individual thunderstorm centers.

2. WHISTLER AND HISS PROPAGATION DIRECTIONS

The fading characteristics of wave electric and magnetic fields resulting from satellite spin have been used in past work to measure the wave normal angles of relatively time-stationary signals, such as hiss, and ground transmitter signals lasting tens of seconds [*Sonwalkar and Inan*, 1986; 1988]. In this study, we advance this method of analysis to permit the measurement of the average wave normal direction of discrete whistlers. Our method is applicable for cases involving a relatively high rate of whistlers.

Experimental Results

The data analyzed covers the time interval from 2104 to 2110 UT on March 24, 1982. At the time shown, the satellite was at $L = 3.8$, geographic latitude and longitude of $\lambda_g = -12°$ and $\phi_g = 23°$, and magnetic latitude of $\lambda = -26°$. The satellite orbit plane was close to the meridional plane. The satellite was spinning with a period of ~6.08 s, the spin axis being perpendicular to the orbit plane. Due to the satellite spin the measured intensity of whistler waves should be subject to periodical variation, as it is conceptually sketched in Figure 1.

The wave data were obtained by the Linear Wave Receiver [*Shawhan et al.*, 1981]. A representative 10 s period of the data is presented in Figure 2. Whistlers ($f > 3$ kHz), as well as plasmaspheric hiss ($f < 3.5$ kHz) were observed from 2104 UT to 2110 UT in way similar to that of shown in Figure 2. Though individual whistler intensities vary, the periodic change in the average amplitude associated with the satellite spin is clearly visible. A narrow band emission seen near 4 kHz occasionally appeared during the period of observation. It exhibits spin fading similar to that for whistlers and hiss and is similar in nature to narrowband emissions previously seen in DE 1 and ISEE 1 satellite data. The wave normal analysis of whistler and hiss signals at 4.5, 3.5, and 2.5 kHz is not affected by the presence of this narrow band signal at ~4.0 kHz. Figure 2 shows that hiss intensity exhibits a drop at frequencies above ~2.9 kHz. A possible mechanism of this cutoff is discussed in the end of Section 3.

To determine the average wave normal angle of whistlers, we measured whistler amplitudes for 147 indentified whistlers in the data at $f = 4.5$ kHz and for 133 whistlers at $f = 3.5$ kHz. Figure 3 shows whistler amplitudes at 4.5 kHz plotted versus the satellite spin phase, with zero phase corresponding to the satellite electric dipole antenna being perpendicular to the Earth's magnetic field. Individual whistler intensities exhibit ~10 dB spread for any fixed satellite spin phase, but the locus of all the measured intensities describes an ellipse as seen in Figure 3.

Figure 4 shows whistler amplitudes at 3.5 kHz plotted in a similar way. There is more spread in the distribution of whistler intensities for this frequency, perhaps due to the relatively high level of the background hiss, which introduced error in our measurements. An elliptical shape is nevertheless evident. Figures 5 and 6 show hiss amplitude versus the satellite spin phase at frequencies 3.5 and 2.5 kHz, respectively. During the observations, the linear wave receiver was operating in 3-6 kHz mode.

Paper number 93JA00662.
0148-0227/93/93JA-00662$05.00

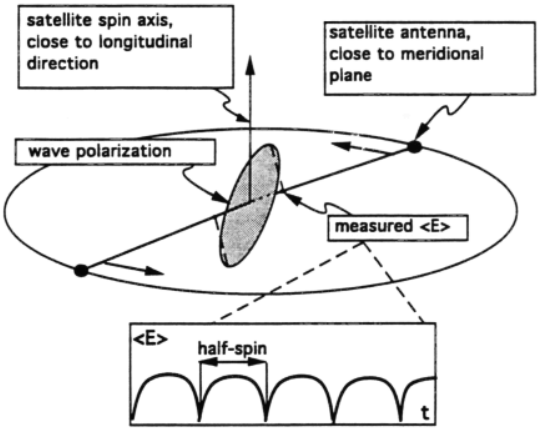

Fig. 1. The geometry of the DE 1 satellite orbit and the electric antenna spin. Whistler wave polarization ellipse is sketched with respect to the antenna orientation. The measured intensity of the wave depends on the relative orientation of the spinning antenna with respect to the wave electric field.

In general, measuring intensities of signals below 3 kHz, filter roll off characteristics (~30 dB/kHz in the 2.2- to 3.0-kHz range) have to be taken into account. However, in the case of wave normal measurements, only relative changes in the signal levels as a function of the satellite spin are important and therefore gain offset due to filter roll off does not affect our results. In the next section we analyze the average wave normal angle of whistlers and hiss based on the fading patterns shown in Figures 3-6.

Theoretical Formulation

An important feature of the data presented in Figure 2 is that nearly all whistlers have the same dispersion pattern corresponding to a direct path from the source to the satellite without any magnetospheric reflections. Based on this observation, we assume that all whistlers have approximately the same wave normal angles. Under this assumption, we derive a relationship determining the whistler intensity as measured by a spinning antenna through the antenna orientation and the actual whistler intensity and the wave normal direction.

Figure 7 shows the coordinate system used. Ambient magnetic field $\vec{B}$ is taken along the z axis, and the electric antenna spin axis $\vec{a}$ is assumed in the z-x plane. The direction of the wavevector $\vec{k}$ is determined by angles ψ and β. In the formulas below we also use (x', y', z') axes, which are defined in such a way that z' is parallel to z and $\vec{k}$ is in (x', z') plane.

If the satellite spins with an angular velocity ω_s, the magnitude of the signal at the antenna terminals for a given frequency is given by

$$E(t) = E_0|(e_1 \cos\beta - e_2 \sin\beta) \sin\omega_s t \cdot \cos\psi_a$$

$$+(e_1 \sin\beta + e_2 \cos\beta) \cos\omega_s t + e_3 \sin\omega_s t \cdot \sin\psi_a| \quad (1)$$

where E_0 is a constant proportional to the actual signal magnitude, time t=0 is chosen as the time when antenna orientation vector $\vec{e}_a$ coincides with y axis, and $e_{1,2,3}$ are components of the complex unit vector of the wave polarization in the x', y', z' system of reference. Expressions for $e_{1,2,3}$ can be obtained as a solution of a system of three linear equations

$$k^2 e_i - \sum_{j=1}^{3} (k_i k_j e_j + \frac{\omega^2}{c^2} \epsilon_{ij} e_j) = 0 \quad (2)$$

where c is the speed of light, $k_1 = k_{x'} = (k_x^2 + k_y^2)^{\frac{1}{2}}$, $k_2 = k_{y'} = 0$, $k_3 = k_{z'} = k_z$; $\epsilon_{ij}(\omega, \vec{k}; \omega_{pe}, \omega_{pi}, \omega_{He})$ is the dielectric tensor of the magnetized plasma [*Krall and Trivelpiece*, 1973] in the same system of reference (x', y', z') where e_i are defined, and $\omega_{pe}, \omega_{pi}, \omega_{He}$ are respectively the electron and ion plasma frequencies and electron gyrofrequency.

For given plasma parameters and angles ψ and β, equation (1) defines the shape of fading of the wave intensity at a frequency ω. The goal of our analysis is to determine values of ψ and β which provide the best fit to the observed fading pattern, which is experimentally measured as a series of amplitude values $E_{ex,j}$ observed at given instants of time t_j. Mathematically, we minimize the value of a function Φ representing the mean squared

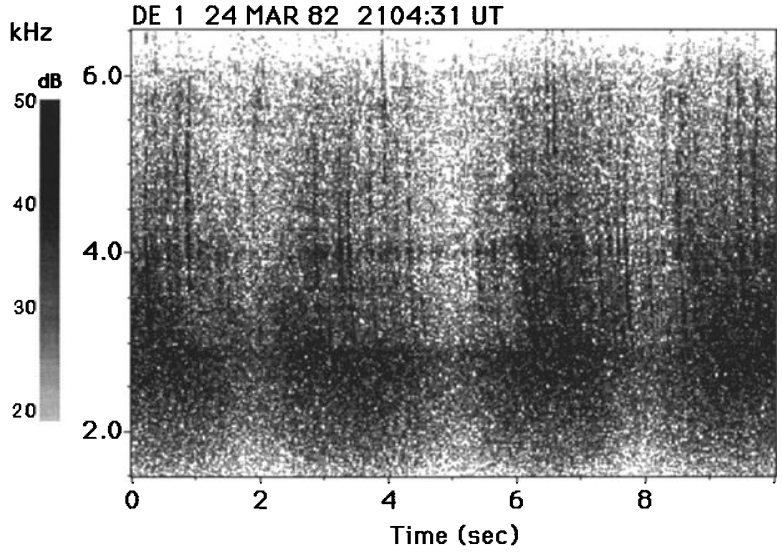

Fig. 2. The spectrogram of the data from the linear wave receiver on the DE 1 satellite. The satellite was at L = 3.8, geographic latitude and longitude of $\lambda_g = -12°$ and $\phi_g = 23°$ respectively, and magnetic latitude of $\lambda = -26°$. Whistlers ($f > 3$ kHz), as well as plasmaspheric hiss ($f < 3.5$ kHz) are seen on the spectrogramm.

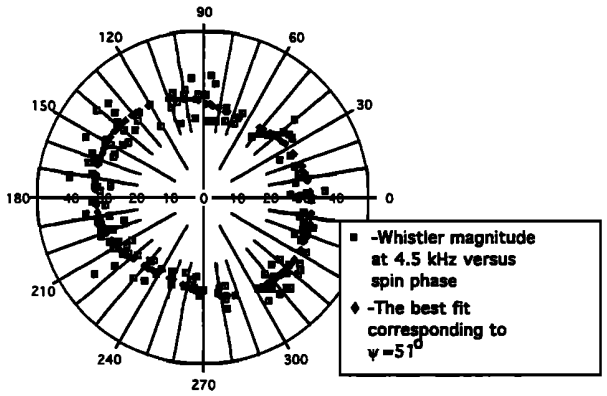

Fig. 3. Amplitudes of 147 individual whistlers measured for f = 4.5 kHz during the time period from 2104 to 2110 UT on March 24, 1982, are shown by squares in decibel scale as a function of the satellite spin phase. The zero angle corresponds to the dipole electric antenna orientation perpendicular to the magnetic field. The best fit theoretically computed values are shown by diamonds, corresponding to the average propagation direction of whistlers at an angle of 51° with respect to the magnetic field and within 20° angle with the magnetic meridional plane.

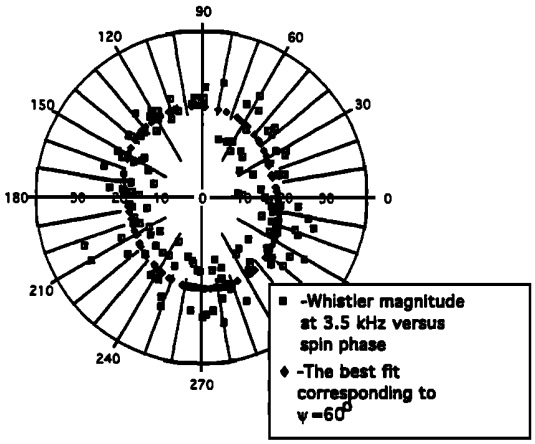

Fig. 4. Amplitudes of 133 individual whistlers measured for f = 3.5 kHz during the same time period as in Figure 3 are shown in the same way. The best fit values to the experimentally observed amplitudes correspond to the average propagation direction of whistlers at an angle of 60° with respect to the magnetic field.

difference between the theoretical fading values $E_j = E(t_j)$ and the experimentally observed values $E_{ex,j} = E_{ex}(t_j)$ at times $t_j (1 \leq j \leq j_{max})$. The function Φ defined as;

$$\Phi(C, \psi, \beta; \omega, \omega_{pe}, \omega_{pi}, \omega_{He}) = \sum_{j=1}^{j_{max}} (20 \log_{10} E_j - 20 \log_{10} E_{ex,j} - C)^2 \quad (3)$$

where C is an unknown normalization constant, $E_{ex,j}$ is a field intensity observed at times t_j in a narrow frequency window centered at ω, and the values of the parameters ω, ω_p and ω_H are assumed to be known. The global minimum value of Φ corresponds to the closest agreement between theoretical values E_j and experimental ones $E_{ex,j}$, in the mean squared sense. This minimum can be found by numerical methods for any set of experimental data $E_{ex,j}$. In the numerical sheme we use the diffusive equilibrium model for the electron plasma density [*Angerami and Thomas*, 1964], and the tilted dipole field model for the magnetic field. Both hiss and whistlers are observed within the plasmasphere, where these models accurately describe the magnetosphere [*Burtis*, 1973].

The value of C which provides a local minimum of Φ for fixed values of ψ and β can be obtained from the relation $\partial\Phi/\partial C = 0$ as

$$C = \frac{1}{j_{max}} \sum_{j=1}^{j_{max}} (20 \log_{10} E_j - 20 \log_{10} E_{ex,j}) \quad (4)$$

In view of the above, the orientation of the wavevector can be determined from experimental data by finding the values of ψ and β which provide the minimum value of Φ, the normalization constant C being defined by (4).

Comparison of Propagation Direction of Whistlers and Hiss

Using this method, we found that the wave normal angles (ψ) of whistlers for the cases shown in Figures 3 and 4 was ~51°

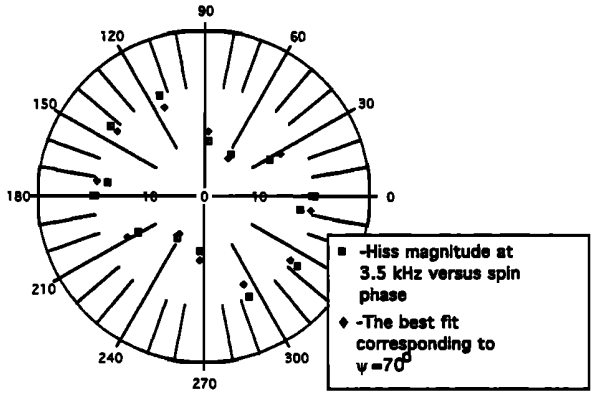

Fig. 5. Amplitude of hiss measured for f = 3.5 kHz during the same time period as in Figures 3 and 4 are shown in the same way. The best fit values to the experimentally observed amplitudes correspond to the average wave vector of hiss at an angle of 70° with respect to the magnetic field, with the perpendicular component tilted at the angle of ~80° with respect to the magnetic meridional plane.

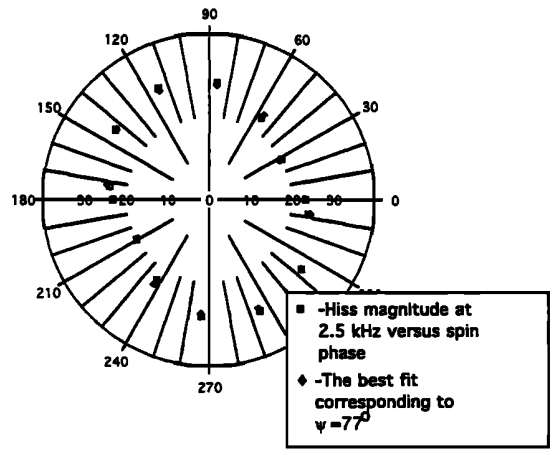

Fig. 6. Amplitude of hiss measured for f = 2.5 kHz during the same time period as in Figures 3 and 4 are shown in the same way. The best fit values to the experimentally observed amplitudes correspond to the average wave vector of hiss at an angle of 77° with respect to the magnetic field, with the perpendicular component tilted at the angle of ~80° with respect to the magnetic meridional plane.

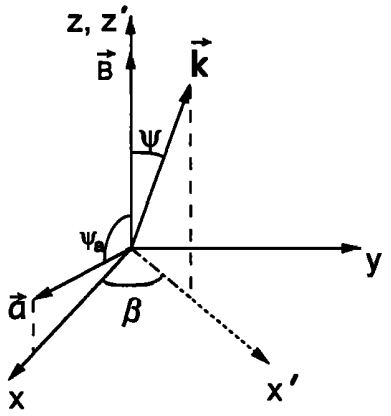

Fig. 7. The frame of reference used in the paper. The magnetic field is parallel to the $\vec{z}$ axis. The satellite spin axis $\vec{a}$ is in the x, z plane, forming an angle of ψ_a with the magnetic field. The magnetic meridional plane is within a few degrees with respect to the y, z plane. The wave vector orientation is characterized by the wave normal angle ψ and azimuthal angle β.

at f = 4.5 kHz and ~60° at f = 3.5 kHz. The corresponding theoretical best fit values E_j versus the satellite phase spin are shown in Figures 3 and 4 as dots on top of experimental values represented by squares. The whistler intensity measurement at 3.5 kHz (Figure 4) exhibited a higher level of the background noise, so that it was not possible to accurately measure the angle between the wave vector and the meridional plane. However, for 4.5 kHz the whistler wave vector was determined to be at an angle of ~20° with respect to the meridional plane.

The wave normal angle of whistlers can be compared to the wave normal angle of plasmaspheric hiss, which was measured to be ~77° at f = 2.5 kHz and ~70° at f = 3.5 kHz, using the same method. Figures 5 and 6 show computed best fit values at 3.5 kHz and 2.5 kHz respectively together with the measured values, in a way similar to Figures 3 and 4. In both cases, the hiss wave vector was nearly perpendicular to the meridional plane, the azimuthal angle of the wave vector tilt with respect to the magnetic meridional plane being ~80°. Figure 8 sketches the wave vectors for whistlers at 4.5 kHz and for hiss at 2.5 kHz as determined from the data, showing that while whistlers propagate at an angle of ~20° with respect to the meridional plane, hiss propagates nearly orthogonal to the same plane, and that whistlers have generally smaller wave normal angles than hiss. The wave vector magnitudes for hiss and for whistlers in Figure 8 are ~2.5 × 10^{-3} m^{-1} and ~1.6 × 10^{-3} m^{-1} respectively.

We can compare the above results with the previous work on the measurement of wave normal angles of signals injected from the Siple Station VLF transmitter [*Sonwalkar and Inan*, 1986]. Experimental parameters in our case (i.e., L value, frequency) are similar to those of Siple Station signals. The wave normal angles for Siple signals observed on DE 1 were found to be ~50–60° with the wave vector being located nearly in the meridional plane [*Sonwalkar and Inan*, 1986], in good agreement with our measurements for whistlers.

Wave normal angles for plasmaspheric hiss have been measured to be generally high [*Lefeuvre et al.*, 1983; *Sonwalkar and Inan*, 1988; *Storey et al.*, 1991]. *Storey et al.*, [1991] have reported wave distribution function analyses in which one, two or three maxima were observed for different wave frequencies and satellite locations. In *Sonwalkar and Inan* [1988] the wave vector of plasmaspheric hiss was found to be at a high angle with respect to the meridional plane, as in the case presented above.

Assuming that whistler rays enter the ionosphere almost along the magnetic field lines, an azimuthal component of the wave vector of whistlers would only arise if there exist considerable density gradients in azimuth. One way that this can happen involves wave scattering from field aligned irregularities, which commonly exist in the ionospheric plasma over a wide range of length scales [*Kelley et al.*, 1980; *Bell and Ngo*, 1990]. Such scattering of initially parallel whistler waves can produce oblique whistler waves with wave vectors of different magnitude distributed in all directions [*Sonwalkar et al.*, 1984]. Depending on the azimuthal component of the wave vector, whistler mode rays would then drift in longitude during their propagation in the magnetosphere. If the observation point (i.e., the satellite) is located at a longitude different from that of ionospheric illumination region by lightning source, only those rays which drift in longitude from the source to the satellite would be observed. Since the direction and magnitude of the longitudinal drift of whistler rays is determined by the azimuthal component of their wave vector, the satellite would observe only those rays for which the azimuthal component of the wave vector has the right polarity.

Since whistler rays continue to drift in longitude after they pass the observation point during their first hop, they will be at a different longitude during their second and consecutive hops, and therefore may not be observed on the satellite. This circumstance may have been in effect in the case of the data presented in Figure 2, where the majority of whistlers corresponded to the direct path of propagation. The fraction of whistlers with greater dispersion (corresponding to either reflected whistlers, or whistlers from a different thunderstorm center) did not exceed a few percent.

The existence of an azimuthal component of the wave normal direction for both whistlers and hiss implies that further assessment of any connection between whistlers and hiss must be based on three-dimensional ray tracing. In the next section, we develop an approximate three-dimensional ray tracing technique, which is then used to show how some plasmaspheric hiss might be produced as a result of nonducted whistler propagation. This idea is qualitatively similar to that presented by *Draganov et al.* [1992] based on two-dimensional ray tracing. Here, we extend the anal-

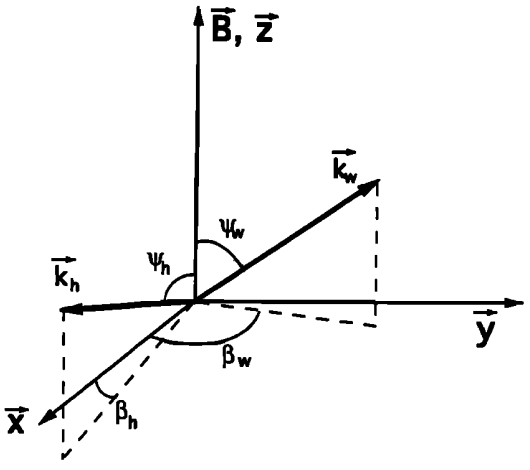

Fig. 8. A sketch showing the orientations of the wave vectors of hiss $\vec{k}_h$ for f = 2.5 kHz and of whistlers $\vec{k}_w$ for f = 4.5 kHz as determined from the data. Note that while whistlers were found to propagate close to the magnetic meridional plane ($\beta_w \sim \pi/2$), hiss propagated at a high angle with respect to the meridional plane.

ysis to three dimensions to account for the fact that plasmaspheric hiss often propagates at a large angle with respect to the meridional plane.

3. WHISTLER WAVE PROPAGATION IN THREE DIMENSIONS

It has been known for some time that the wave vector of nonducted whistlers approaches the resonance cone after the first several magnetospheric reflections [*Edgar*, 1976, and references therein]. On the basis of ray tracing calculations, it was shown recently that magnetospherically reflected whistlers can produce some plasmaspheric hiss [*Draganov et al.*, 1992], a model consistent with the observed high wave normal angles for plasmaspheric hiss. The ray tracing study of hiss generation in the work by *Draganov et al.* [1992] was performed using a two-dimensional numerical model, assuming that both the wave vector and the wave trajectory lie in the magnetic meridional plane. As we see from the wave normal analysis above, this assumption is difficult to justify. Therefore, comprehensive modeling of nonducted whistler propagation and its role in the establishment of plasmaspheric hiss should include three-dimensional effects. Accurate three-dimensional ray tracing problem is complicated and in general can be performed only by computationally intensive numerical methods [*Green et al.*, 1977; *Cairó and Lefeuvre*, 1986] which do not easily lend themselves to analysis of a large number of ray-paths. In the case of multiple magnetospheric reflections, as the wave vector approaches the resonance cone

$$\psi \rightarrow \psi_r \sim \cos^{-1}\sqrt{\frac{\omega^2}{\omega_{pe}^2}+\frac{\omega^2}{\omega_{He}^2}-\frac{\omega_{pi}^2}{\omega_{pe}^2}},$$

the numerical solutions can become unstable. On the other hand, in this regime when $\psi \sim \psi_r$, considerable analytical simplifications can be made. In this section, we derive approximate equations for three-dimensional propagation of whistler waves with wave vectors close to the resonance cone. These equations are then used to investigate the generation of plasmaspheric hiss via multiple reflections of nonducted whistlers.

Analytical Formulation

We start from the approximate dispersion equation for quasi-electrostatic whistler wave in cold plasma, obtained from Maxwell equations and equations of motion for the electron and ion species [*Krall and Trivelpiece*, 1973]

$$D(\omega,\vec{k}) = -1+\frac{\omega_{pi}^2}{\omega^2}+\frac{\omega_{pe}^2}{\omega^2}\cos^2\psi-\frac{\omega_{pe}^2}{\omega_{He}^2}=0 \qquad (5)$$

Here $\cos\psi = k_\parallel/k$, $\omega_{pe,i}$ are plasma electron and ion frequencies repectively, ω_{He} is electron gyrofrequency, and $k_\parallel$ is the wave vector component parallel to the ambient magnetic field. Since we are primarily interested in wave propagation at high altitudes, we consider only cold hydrogen plasma. The equations for the ray trajectory in the inhomogeneous plasma can be obtained in parametric form as $\vec{k} = \vec{k}(\tau)$, $\vec{r} = \vec{r}(\tau)$, $t = t(\tau)$ by differentiating the function $D(\omega,\vec{k})$:

$$\frac{d\vec{k}}{d\tau} = \frac{\partial D(\omega,\vec{k})}{\partial \vec{r}} \qquad (6a)$$

$$\frac{d\vec{r}}{d\tau} = -\frac{\partial D(\omega,\vec{k})}{\partial \vec{k}} \qquad (6b)$$

$$\frac{dt}{d\tau} = \frac{\partial D(\omega,\vec{k})}{\partial \omega} \qquad (6c)$$

We start our analysis of equations (6) by evaluating the right-hand side of equation (6*c*). After taking the derivative of $D(\omega,\vec{k})$ with respect to ω, we use the fact that $D(\omega,\vec{k}) = 0$ along the trajectory to obtain

$$\frac{dt}{d\tau} = -\frac{2}{\omega}\left(1+\frac{\omega_{pe}^2}{\omega_{He}^2}\right) \qquad (7)$$

Since for typical plasmaspheric parameters $\frac{\omega_{pe}^2}{\omega_{He}^2} \gg 1$, we have

$$\frac{dt}{d\tau} = -\frac{2}{\omega}\frac{\omega_{pe}^2}{\omega_{He}^2} \qquad (8)$$

From equations (6*b*), and (8) we can derive expressions for the wave group velocity

$$v_{g\perp} = \frac{dr_\perp}{d\tau}\left(\frac{dt}{d\tau}\right)^{-1} = -\frac{\omega_{He}^2}{\omega}\frac{k_\parallel^2 k_\perp}{k^4} \qquad (9a)$$

$$v_{g\parallel} = \frac{dr_\parallel}{d\tau}\left(\frac{dt}{d\tau}\right)^{-1} = \frac{\omega_{He}^2}{\omega}\frac{k_\parallel k_\perp^2}{k^4} \qquad (9b)$$

Note that expressions for $v_{g\perp}, v_{g\parallel}$ include $k_\parallel, k_\perp$, the values of which can be determined from equation (6*a*). In calculating the derivatives with respect to $\vec{r}$ in (6*a*), we take into account the dependence of $D(\omega,\vec{k})$ on the coordinates $\vec{r}$ through the parameters $\omega_{pe}, \omega_{pi}, \omega_{He}$ of the inhomogeneous media. A first simplification of equation (6*a*) can be made by separately evaluating the contributions from the inhomogeneity of the plasma density and the inhomogeneity of the magnetic field. Since along the trajectory $D(\omega,\vec{k}) = 0$, it can readily be shown that the contribution to equation (6*a*) due to the inhomogeneity in density is

$$\left(\frac{\partial D(\omega,\vec{k})}{\partial \vec{r}}\right)_n = \frac{1}{n}\frac{\partial n}{\partial \vec{r}} \qquad (10)$$

whereas that due to inhomogeneity of the magnetic field is

$$\left(\frac{\partial D(\omega,\vec{k})}{\partial \vec{r}}\right)_H = \frac{2}{H}\frac{\omega_{pe}^2}{\omega_{He}^2}\frac{\partial H}{\partial \vec{r}} \qquad (11)$$

Since for typical plasmaspheric parameters

$$\frac{\omega_{pe}^2}{\omega_{He}^2} \gg 1,$$

we have

$$\left(\frac{\partial D(\omega,\vec{k})}{\partial \vec{r}}\right)_H \gg \left(\frac{\partial D(\omega,\vec{k})}{\partial \vec{r}}\right)_n.$$

This approximation means that the ray trajectory is primarily determined by the magnetic field inhomogeneity, rather than by the density inhomogeneity. In the derivation we assumed that the density profile does not have any abrupt changes along the ray trajectory (e.g., the wave does not encounter ducts or the plasmapause during the propagation).

We use the approximation above to determine the radial component k_r of the wave vector in the spherical coordinate system associated with the earth magnetic field. Since we only have to evaluate the derivative with respect to the magnetic field, and since the magnetic field intensity is proportional to the inverse third power of radial distance (dipole approximation), we have

$$\left(\frac{d\vec{k}}{d\tau}\right)_r = -\frac{\omega_{pe}^2}{\omega_{He}^2}\frac{6}{r} \qquad (12)$$

where r is radial distance to the ray location. Substituting $dt/d\tau$ from (8), we get a surprisingly simple equation for $(d\vec{k}/d\tau)_r$

$$\left(d\vec{k}/dt\right)_r = \left(\frac{d\vec{k}}{d\tau}\right)_r\left(\frac{dt}{d\tau}\right)^{-1} = 3\frac{\omega}{r} \qquad (13)$$

Now we turn to the evaluation of the left-hand side of (13). In an earth centered spherical coordinate system, the direction of unit vectors depend on the ray location. Therefore,

$$\left(\frac{d}{d\tau}(\vec{e}_r k_r + \vec{e}_\theta k_\theta + \vec{e}_\phi k_\phi)\right)_r = \frac{dk_r}{d\tau} + k_r\left(\frac{d\vec{e}_r}{d\tau}\right)_r + k_\theta\left(\frac{d\vec{e}_\theta}{d\tau}\right)_r + k_\phi\left(\frac{d\vec{e}_\phi}{d\tau}\right)_r \quad (14)$$

We can estimate the relative contribution of different terms in the right-hand side of (14). The second term is identically equal to zero. The fourth term is typically much less than the third one, since ray propagation is typically in the θ direction so that the e_ϕ change is smaller. Thus only contributions from the first and the third terms must be estimated. The contribution from the third term can be evaluated as

$$k_\theta\left(\frac{d\vec{e}_\theta}{d\tau}\right)_r \simeq k_\theta\left(\frac{d\vec{e}_\theta}{d\theta}\right)_r \frac{d\theta}{d\tau} = k_\theta \frac{d\theta}{dt}\frac{dt}{d\tau} \simeq \frac{k_\| v_{g\|}}{r}\frac{\partial D}{\partial \omega} \quad (15)$$

where we again assume that ray propagation occurs primarily in θ direction, which is close to the direction of the magnetic field lines for a typical magnetospherically reflected whistler ray. We substitute in (15) the value of $v_{g\|}$ from (9*b*) and $\partial D/\partial\omega$ from the right-hand side of (8) to get

$$k_\theta\left(\frac{d\vec{e}_\theta}{d\tau}\right)_r \simeq \frac{2}{r}\frac{k_\|^3 k_\perp}{k^4}\frac{\omega_{pe}^2}{\omega^2} \quad (16)$$

For typical parameters of whistler rays considered here the dispersion equation gives

$$\left(\frac{k_\|}{k}\right)^2 < \left(\frac{\omega}{\omega_{He}}\right)^2$$

Substituting in (16) along with $k_\perp/k < 1$, we get

$$k_\theta\left(\frac{d\vec{e}_\theta}{d\tau}\right)_r < \frac{2}{r}\frac{k_\|}{k}\frac{\omega_{pe}^2}{\omega_{He}^2} \quad (17)$$

Comparing this formula to the right-hand side of (12), we see that for highly oblique whistler waves ($k_\| \ll k$), the evaluated term $k_\theta\left(\frac{d\vec{e}_\theta}{d\tau}\right)_r$ makes a negligibly small contribution in (13,14). Therefore we can rewrite equation (13) as

$$\frac{dk_r}{dt} = 3\frac{\omega}{r} \quad (18)$$

Since magnetic field gradients in the azimuthal direction are small compared to those in the radial and θ directions, the azimuthal component k_ϕ of the wave vector satisfies the conservation law

$$k_\phi r^2 \sin\theta = \text{ const} \quad (19)$$

Since the direction of the magnetic field line is known for any given point, all three components of the wave vector can be determined from k_r, k_ϕ, and the following expression for $k_\|/k$ ratio obtained from (5)

$$\frac{k_\|^2}{k^2} = \frac{\omega^2}{\omega_{pe}^2}\left(1 + \frac{\omega_{pe}^2}{\omega_{He}^2} - \frac{\omega_{pi}^2}{\omega^2}\right) \quad (20)$$

Therefore equations (18) through (20), and the known magnetic field line direction and plasma parameters fully determine the wave vector at any point along the ray trajectory. Though equations (9) specify only two quantities, all three components of the group velocity can be determined by using the fact that the group velocity vector is perpendicular to the wave vector and lies in the same plane with the wave vector and the ambient magnetic field. Therefore the set of equations (9, 18-20) fully define the ray trajectory and can be easily solved numerically.

Equations (9) and (18)-(20) have a scaling property in that they remain valid upon substitution of $\vec{k} = \alpha\vec{k}', t = \alpha t'$ noting that $\vec{v} = d\vec{r}/dt$. In other words, two rays originating at the same point with the same frequency and wavenormal angle, but with different magnitudes of wavevectors, propagate along the same trajectory, but with different group velocities, a result consistent with numerical ray tracing. This scaling property is valid within the used above quasi-electrostatic approximation, when a large spread in wave vector magnitudes corresponds to a small spread in wave normal angles.

An interesting feature of (9) and (18)-(20) can be observed if we substitute $k_\|$ from (20) to (9*b*). Since $k_\|$ has a real value only between the points of magnetospheric reflections, and is equal to zero at these points, the resulting equation for $v_\|$ looks like an equation for a nonlinear oscillation of a particle in a potential well, where the expression for the potential includes $k, \omega_{pe}, \omega_{pi}, \omega_{He}$ as parameters. The period of the oscillations depends on the second derivative of the pseudopotential along the field line. Since k grows in accordance to equation (18), one can show that the potential well becomes more and more shallow, and therefore the period of the ray oscillations grows with time, in agreement with results from exact numerical solution for whistler ray trajectories.

Numerical Results

Numerical solution of (9) and (18)-(20) were carried out using a diffusive equilibrium model for the plasmaspheric electron density [*Angerami and Thomas*, 1964] with a plasma density of 500 cm^{-3} at L=4. The earth's magnetic field was taken to be that of a tilted dipole. Test comparison in a selected case showed excellent agreement between the approximate ray tracing technique and the exact 3D solution obtained using a 3D raytracing program. The typical trajectory of quasi-electrostatic whistler waves bounces between LHR reflection surfaces (defined as surfaces where the wave frequency is equal to the local lower hybrid resonance frequency) while the average trend is characterized by an azimuthal drift and an asymptotic decrease in L shell with time. The magnitude of the wave vector steadily grows in accordance with (18). The lifetime of quasi-electrostatic whistler mode waves in the magnetosphere can be estimated using (18), since when the wave vector is sufficiently large, the parallel component of the wave velocity becomes small enough for Landau damping to be significant. Landau damping is negligible if

$$\mathcal{E} = \frac{m}{2}\left(\frac{\omega}{k_\|}\right)^2 \gg E_{th} \quad (21)$$

where E_{th} is the electron thermal energy. Substituting $k_\|$ from (20) and $k \sim k_r$ from (18), and conservatively using $\mathcal{E}$ = 20 eV, the lifetime of a 2.5-kHz wave propagating at $L \sim 4$ is estimated as $t_{max} > 20$ s. The lifetimes for lower-frequency waves propagating at lower L shells can be substantially larger, up to $\sim 10^2$ s for a 1 kHz quasi-electrostatic whistler propagating at $L < 3$, in agreement also with numerical 2D ray tracing calculations [*Draganov et al.*, 1992].

Figure 9 shows L values and drift in magnetic longitude $\Delta\phi$ for the first 5 equatorial plane crossings of a 2.5 kHz ray originating at a magnetic latitude of $\lambda = 45°$. The initial wave vector was chosen to be $k = 0.75 \times 10^{-2}$ m^{-1}, with its perpendicular component oriented at 135° angle with respect to the radial direction. The azimuthal component of the wave vector under this condition was $k_\phi = k\cos 135° \sim 5 \times 10^{-3}$ m^{-1}. The electron Landau resonance energy $\mathcal{E} = m/2(\omega/k_\|)^2$ along the trajectory was determined numerically, and it was well above the thermal plasma energy for the first three equatorial plane crossings with

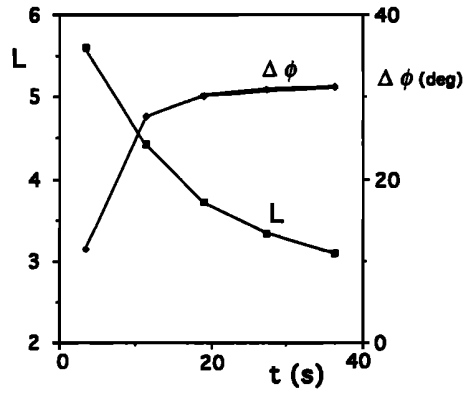

Fig. 9. L values and longitudinal drift $\Delta\phi$ of a 2.5-kHz quasi-electrostatic whistler mode ray in the magnetosphere. The initial magnitude of the wave vector (k = 0.75 m^{-2}) was chosen so as to provide a group time delay of ~20 s at the third hop.

$\mathcal{E} > 20$ eV, in general agreement with our analytical estimations. We note that the third hop of the wave propagated at $L \simeq 3.8$, i.e., where the observations reported in Figure 2 were made. The initial magnitude of the wave vector was chosen so as to provide a group time delay of ~20 s. Rays with considerably greater initial values of k would be damped earlier and would not reach L = 3.8. However, rays originating from the same point and with the same frequency, but with smaller initial magnitude of the wave vector may propagate even further, executing the fourth and subsequent hops. As predicted by the scaling feature of (9) and (18)-(20), such rays would follow the same trajectory with smaller group delays. Figure 10 shows the range of group delays of the rays with different initial wave vectors in the range $k_{min} < k < k_{max}$ at their third crossing of the equatorial plane at L=3.8. Smaller group delays of order of several seconds correspond to small initial magnitudes of the wave vector, where the quasi-electrostatic approximation is not valid, and are sketched by a dashed line.

The direction of propagation of whistler waves as observed at any point in the magnetosphere is determined by the propagation path of the wave energy from the source region to the observation point. Although whistler waves may initially have different wave vector orientations as a result of scattering from plasma irregularities, they may have approximately the same wave vector directions as observed on a satellite. Figure 11 shows positions of the third equatorial crossing of 2.5 kHz whistler rays with different initial wave vector directions as computed using our three-dimensional ray tracing model. The magnitude of the wave vector and the initial position of the rays are the same as in Figure 9. We see that rays originating at the same point with different initial azimuthal wave vector orientations can be observed at different L-shells and different longitudes. For example, if a satellite is located at ~25°-30° away in longitude from that of the source (e.g., thunderstorm) location, third-hop whistler rays should initially have azimuthal wave vector directions of ~120-140° in order to be observable on the satellite. Ray tracing calculations show that such rays would still have significant azimuthal wave vector components at the observation point in spite of the tendency for wave vectors to "collimate" near the magnetic meridional plane as shown by three dimensional ray tracing calculations [*Cairó and Lefeuvre*, 1986]. The plasmaspheric hiss shown in Figure 2 does exhibit finite azimuthal wave vector component, consistent with its having been produced by whistlers originating in thunderstorm centers at longitudes different from that of the observation point.

Figure 11 shows that magnetospherically reflected whistlers, which potentially may produce hiss, populate a limited region of the magnetosphere (assuming that they originate from the same thunderstorm center). Since the group velocity direction depends on the wave frequency, the shape and dimensions of the regions of magnetosphere populated by whistler wave energy should also depend on the wave frequency. Ray-tracing calculations show that whistler rays with higher frequencies propagate along trajectories qualitatively similar to those of lower frequency rays, but located at lower altitudes. For example, the points of the third equatorial crossing of 3.5 kHz rays are at $\Delta L \sim 0.6$ below those shown in Figure 11 for 2.5 kHz rays (all other parameters being the same). If the observation point is located in a region of the plasmasphere which is accessible for whistler rays from only a limited frequency band, hiss produced by whistlers and observed on a satellite may exhibit higher- and/or lower-frequency cutoffs, like that at ~2.9 kHz in Figure 2.

In our approximate analytical model, the wave group velocity is inversely proportional to the wave vector magnitude, and its direction is exactly perpendicular to the resonance cone surface.

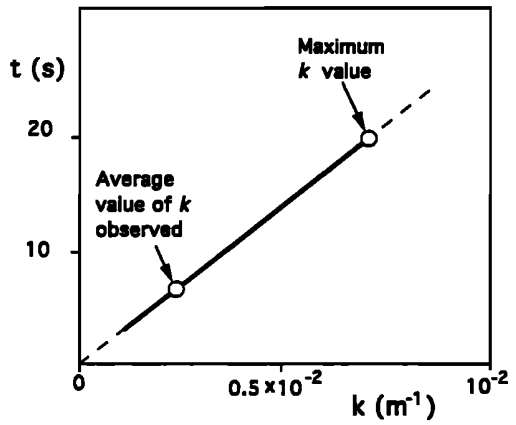

Fig. 10. Group delays and wave vectors of the third hop 2.5-kHz whistler rays as observed at L=3.8 in the magnetosphere. Maximum value of the wave vector k corresponds to the largest delay and is limited by Landau damping of the wave. The measured average magnitude of the wave vector for hiss corresponds to about one third of the maximum possible value and is shown by an arrow. Our analytical formulas are not valid for for small k, t values; this section is shown in a dashed line.

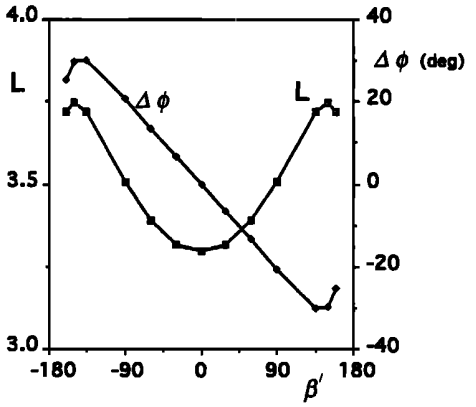

Fig. 11. L values and longitudinal drift $\Delta\phi$ of 2.5-kHz whistler mode rays at the third equatorial crossing versus their initial azimuthal angle β' between the perpendicular component of the wave vector and the magnetic meridional plane. The value of β' is within a few degrees of the value of the angle between axes x' and y in Figure 7.

We can estimate the validity of this quasi-electrostatic approximation in our case by comparing the resonance cone angles to the wave normals as measured for plasmasheric hiss. Assuming the dipole model for the magnetic field, the resonance cone angles can be estimated as $\psi_r \sim 77°$ for $f = 3.5$ kHz and $\psi_r \sim 81°$ for $f = 2.5$ kHz. Since hiss wave normal angles were measured to be $\sim 70°$ and $\sim 77°$ respectively, they appear to be within few degrees from the resonance cone. Test comparisons of results from our approximate model with full cold plasma theory show that, for the parameters used here, our method is accurate to within $\sim 5°$ for the direction and $\sim 20\%$ for the magnitude of the wave group velocity. The error of $\sim 20\%$ is of the same order as that resulting from the uncertainty of the wave vector measurement, so that our approximate analytical ray tracing formulation is sufficiently accurate for the interpretation of the experimental data in hand.

4. DISCUSSION

In this section we discuss (1) the spatial, temporal and directional association between whistlers and hiss in view of the results of previous sections and (2) revisit the issue of sustenance of hiss energy by lightning as suggested by *Draganov et al.* [1992].

Association of Hiss With Lightning and Whistlers

An important feature of the results presented in Figure 9 is that the longitude drift of whistler mode rays is limited to $\sim 30°$, which indicates that the group velocity lies almost in the magnetic meridional plane during the fourth and subsequent hops. Since the wave group velocity lies in the same plane as the wave vector and the magnetic field, this would in turn mean that the wave vector lies in the meridional plane. From a qualitative point of view this result can be explained as the growth of the radial component of the wave vector (see equations (18) and (19)). After several tens of seconds, the radial component of the wave vector becomes large enough to tilt the wave vector toward the meridional plane, regardless of the initial value of the azimuthal component. This behaviour of whistler rays is in agreement with the "collimation effect" for azimuthal angles of whistler propagation directions [*Cairó and Lefeuvre*, 1986].

It is useful to compare the results of the ray-tracing study presented here to those of [*Draganov et al.*, 1992], where two-dimensional propagation of nonducted whistlers with a narrow distribution of initial wave normal angles were studied. Draganov et al. found that over time periods of as much as $\sim 10^2$ s, the whistler wave vectors tilted toward the resonance cone due to the magnetic field and plasma density gradients, and the resulting quasi-electrostatic whistler rays merged into a noise-like emission similar to hiss. The two-dimensional analysis of Draganov et al. showed that plasmasheric hiss may be produced by whistler propagation at frequencies not too much higher than the local lower hybrid frequency. The results of our three-dimensional ray tracing of quasi-electrostatic waves indicate that wave frequencies do not need to be restricted to the vicinity of the LHR frequency if the wave vector has a significant initial azimuthal component. Although the existence of a azimuthal wave vector component is not necessary for hiss generation by whistlers, our model predicts that hiss should have a azimuthal wave vector component at frequencies well above the local lower hybrid frequency.

Since the longitudinal drift of whistler mode waves is apparently limited, plasmaspheric hiss should be observed within $\pm 30°$ in longitude of its source. If hiss is generated by lightning, there should thus be a correlation between the distribution of the average plasmaspheric hiss intensity in longitude and the geographic regions of high thunderstorm activity. If hiss is generated primarily by energetic particles, its intensity should exhibit weak dependence on longitude, except during periods immediately after substorms, when the injected population of energetic particles is longitudinally dependent. A comprehensive survey of hiss intensity at low altitudes was recently reported [*Parrot*, 1990]. While the statistical data presented show prominent maxima of hiss intensity at longitudes of high thunderstorm activity ($\sim 250°$E$-320°$E) [see *Parrot*, 1990, and references therein], the relevance of this result to the problem in hand is not clear since most hiss, and in particular that which evolves from magnetospherically reflected whistlers would be confined to higher altitudes.

The measurements of hiss propagation direction presented above show a local azimuthal anisotropy of hiss propagation directions. In general, azimuthal component of the hiss wave vector can be formed only if there is an azimuthal anisotropy of the hiss source location and/or azimuthal anisotropy of energetic particle distribution which might generate plasmaspheric hiss. While lightning activity as a possible source of hiss obviously has an azimuthal dependence, the distribution of the energetic particles in the magnetosphere is generally less dependent on longitude, with the exception of time periods immediately after magnetic storms, when injection of energetic particles takes place. For the case discussed in this paper relatively quiet ($\Sigma K_p \sim 15$-20) conditions prevailed, so that it is reasonable to assume only weak variation of the energetic particle distribution in longitude. Thus, the fact that there was indeed an azimuthal component of hiss wave normal angle in this case is consistent with hiss generation by whistlers, rather than generation by energetic particles.

For oblique propagation and multiple magnetospheric reflections, the spread in group delays of signals originating at the same point below the ionosphere and observed at a fixed location (i.e., satellite) in the magnetosphere may be up to 20 s or more, according to Figure 9. This theoretical prediction may be manifested in satellite data, which show hiss-like signals lasting for $\sim 10 - 20$ s after the observed whistlers in the magnetosphere [*Sonwalkar and Inan*, 1989]. *Sonwalkar and Inan* [1989] ascribed this phenomena to the embryonic triggering of hiss by whistlers. While we do not reject the possibility of hiss amplification via wave-particle interaction, we note that the duration of the hiss-like signals observed after whistlers appear to be solely explainable by propagation effects alone. Since whistler rays at higher frequencies are damped after a shorter time, our proposed mechanism would lead to a higher frequency cutoff in the hiss following whistlers, with lower frequencies lasting longer, precisely as observed in the experiment [*Sonwalkar and Inan*, 1989]. Another example of the same effect may be data presented by *Bell et al.* [1981], showing up to 10-20 s delays of arrival of multiply reflected pulses from ground-based transmitters observed on the ISEE-1 satellite.

Since rays with different wave vectors are observable at any point, our analysis of the spin fading characteristics provides an "average" value of the magnitude of the wave vector. This average value must necessarily be less than the maximum possible value of k as limited by the Landau damping condition discussed above. The average value of k corresponds to some average value of group delay, which must in turn be less than the maximum group delay estimated as ~ 20 s at the third hop and shown with an arrow in Figure 10. Since the observed magnitude of k was $\sim 2.5 \times 10^{-3}$ m^{-1}, i.e., about one third of the estimated maximum possible value, the average group delay should also be about one third of the maximum, i.e., ~ 7 s. Therefore, at the observation

point one can simultaneously observe signals from all whistlers originating up to at least 7 s before the time of the observation. Due to an extremely high whistler rate in the case analyzed here, there were several tens of whistlers during a 7-s period, each of them potentially contributing to the observed plasmaspheric hiss. Signals from different whistlers lasting on average for ~7 s each, would overlap and completely lose their initial discrete character. Thus, it is quite reasonable that the plasmaspheric hiss shown in Figure 2 might have been produced entirely by nonducted oblique whistlers.

While propagating through the ionosphere, whistler wave energy may be split between scattered quasi-electrostatic waves and nonscattered electromagnetic waves. As we show in this paper, quasi-electrostatic waves may form hiss on time scales of ~7 s due to the spread in their velocity of their propagation. Nonscattered whistler rays would propagate without any significant spread in group delay, and therefore would be observed as discrete whistlers on a satellite. Observed cases of discrete whistlers superposed on hiss (Figure 2) may be a manifestation of such a split of whistler energy. For discrete whistlers which have not scattered during their propagation to the observation point, the wave vector orientation would be determined solely by magnetic field and plasma density gradients, and the wave vector would not significantly deviate from the meridional plane, in agreement with our measurements. Upon further propagation, the wave vectors of discrete whistler would approach the resonance cone, so that on longer time scales (~10^2 s) their low-frequency components may also evolve into plasmasheric hiss [*Draganov et al.*, 1992].

Sustenance of Hiss Energy by Lightning

While the data presented show that some plasmaspheric hiss may be produced by multiply reflected whistlers, additional work has to be done in order to investigate what fraction of hiss is indeed produced by lightning on a global scale. The first attempt to address this issue was made in previous work by *Draganov et al.* [1992], where it was stated that lightning generated whistlers provide enough energy to sustain hiss on a global scale. Wave vector values used in [*Draganov et al.*, 1992] were based entirely on results from a two dimensional ray tracing calculation, and the formulas used for the hiss wave energy contained an error (the value of the angle between the electric field and the wave vector was used instead of the angle between the electric and magnetic field). Below, we provide the energy estimations, based on k values from the actual wave vector measurements and also accounting for 3D propagation.

To estimate the total hiss energy, we start from the formula for the energy density (per unit volume) of the oblique whistler mode wave

$$q_h = \frac{B_h^2}{\mu_0} \frac{c}{v_g} \frac{1}{n_h \sin\alpha} \tag{22}$$

where B_h is the total wave magnetic field, n_h is the refractive index and α is the average angle between the electric field of the wave and the wave vector. The latter two parameters can be estimated through a solution of the dispersion equation for the oblique whistler wave [*Krall and Trivelpiece*, 1973]. The numerical solution of the dispersion equation leads to

$$\frac{c}{v_g} \frac{1}{n_h \sin\alpha} \sim 1$$

for typical magnetospheric parameters and for k values of $\sim 2 \times 10^{-3} - 7 \times 10^{-3}$ m^{-1} as obtained above. We note that for the same wave magnetic field intensity, the hiss energy density would be higher for larger k, since for large k the wave becomes more electrostatic, and a larger fraction of its energy is concentrated in the electric field, which is not measured by the magnetic antenna. Quantitatively, this effect would manifest itself as lower values of $\sin\alpha$ in (22).

We use the hiss energy density to estimate the total rate of energy loss of the hiss wave in the magnetosphere as $Q_h = q_h V/\tau_h$, where $V \sim 2 \times 10^{22}$ m^3 is the total volume of the magnetosphere occupied by hiss, and τ_h is the lifetime of the whistler waves in the magnetosphere. Though the particular case analyzed in this paper refers to relatively high hiss frequencies (f~2-3 kHz), the major concentration of hiss energy is typically at or near ~1 kHz [*Thorne et al.*, 1973]. As it was shown by *Draganov et al.* [1992], nonducted whistlers may evolve into plasmaspheric hiss at frequencies of order of 1 kHz after several tens of magnetospheric reflections in a way similar to that described in this paper. On this basis, we choose to make comparison of hiss and whistler energy densities by using observed hiss spectral densities at ~1 kHz. We adopt the value of ~1 pT/Hz$^{1/2}$ in a 300 Hz frequency band as reported by *Thorne et al.* [1973]. Substituting τ_h ~20 s, we get $Q_h \sim 3 \times 10^5$ J/s.

We compare this value to the total energy input from whistlers into the magnetosphere, which can be estimated as

$$Q_w = \frac{B_w^2}{\mu_0} \frac{c}{n_w} S \tau_w R \tag{23}$$

where B_w is the whistler wave amplitude, n_w is the refractive index, τ_w is the whistler duration at the equatorial plane, S is the area illuminated by an average whistler in the equatorial plane, and R is the global rate of lightning discharges. The latter parameter can be estimated as $R \sim 10^2$ s^{-1} [*Uman*, 1987, p. 46]. Though the area illuminated by a whistler can be significantly larger than the magnetospheric projection of the spot of whistler entrance in the ionosphere due to azimuthal drift of whistler rays, we conservatively neglect the azimuthal divergence of whistler rays in our estimates. Taking the azimuthal dimension of the whistler illumination region at the lower ionosphere to be ~2000 km, and assuming that whistler rays cross the equatorial plane in $2 < L < 4$ (as it follows from ray tracing calculations), we estimate $S \sim 6 \times 10^7$ km^2. For a whistler wave amplitude of ~3 pT (consistent with satellite observations [*Sulić et al.*, 1991]), refractive index of ~30, and typical duration of ~0.3 s we estimate the whistler wave energy input into the magnetosphere to be $Q_w \sim 2 \times 10^5$ J/s. Since Q_w is comparable to Q_h, lightning-generated whistlers can indeed provide a significant portion of energy to maintain the 1 pT/Hz$^{1/2}$ on a global scale. Our mechanism of hiss generation does not rule out the possibility of wave amplification due to wave-particle interactions [*Church and Thorne*, 1983], so that the observed intensity levels of the plasmaspheric hiss may be a result of both hiss generation by non-ducted whistlers and its subsequent amplification by the interaction with energetic electrons. We note that our ray tracing calculations in fact show that the whistler wave energy from lightning discharges should be inhomogeneously distributed in longitude, exhibiting correlation with thunderstorm activity. Therefore, while our energy estimates are based on azimuthally averaged values, the local values of both hiss energy density and lightning generated whistler energy might be significantly different.

5. SUMMARY

We have reported the first simultaneous measurement of the propagation direction of discrete whistlers (originating in lightning and arriving at the satellite over a short direct path) and

plasmaspheric hiss as observed on the DE 1 satellite. The whistler wavenormal angles and dispersion characteristics were consistent with propagation over typical nonducted magnetospheric paths with propagation being at 50° – 60° with respect to the magnetic field and within < 20° with respect to the meridional plane. The wave normal angles for hiss were found to be larger, being 70° – 77°, consistent with previous suggestions that some plasmaspheric hiss may consist of a superposition of many multiply reflected whistlers [*Draganov et al.*, 1992]. The azimuthal angles of the wave vector for hiss were found to be at an angle of ~80° with respect to the magnetic meridional plane.

The fact that both whistlers and hiss propagation directions have significant components in azimuth indicate that considerations of three dimensional ray propagation would be important in assessing the possible causative connection between whistlers and hiss. An approximate analytical model was put forth to evaluate the propagation of quasi-electrostatic whistlers in three dimensions. Applications of the model indicate that waves injected from fixed thunderstorm centers on the ground may drift in longitude by as much as ±30° during their multiply reflected propagation in the magnetosphere. Considerations of group delay and overlap of many such waves lend support to the concept of formation of magnetospheric hiss as a superposition of magnetospherical reflected whistlers.

We have also reevaluated the possibility of the sustenance of hiss by wave energy injected from lightning. Our estimates indicate that lightning generated whistlers can provide a significant portion of the energy needed to maintain the 1 $pT/Hz^{1/2}$ average intensity of hiss on a global scale.

Acknowledgments. We thank our colleagues in the STAR Laboratory for helpful discussions. This research was supported by NASA grant NAG5-476 to Stanford University.

The Editor thanks M. Parrot and another referee for their assistance in evaluating this paper.

REFERENCES

Angerami, J. J., and J. O. Thomas, Studies of planetary atmosphere, 1, The distribution of electrons and ions in the Earth's exosphere, *J. Geophys. Res.*, *69*, 4537, 1964.

Bell, T. F., and H. D. Ngo, Electrostatic lower hybrid waves excited by electromagnetic whistler mode waves scattering from planar magnetic-field-aligned plasma density irregularities, *J. Geophys. Res.*, *95*, 149, 1990.

Bell, T. F., and U. S. Inan, ISEE-1 observations in the magnetosphere of VLF emissions triggered by nonducted coherent VLF waves during VLF wave-injection experiments, *Adv. Space Res.*, *1*, 203, 1981.

Burtis, W. J., Electron concentrations calculated from the lower hybrid resonance noise band observed by OGO-3, *J. Geophys. Res.*, *78*, 5736, 1973.

Cairó, L., and F. Lefeuvre, Localization of sources of ELF/VLF hiss observed in the magnetosphere: three-dimensional ray tracing, *J. Geophys. Res.*, *91*, 4352, 1986.

Church, S. R., and R. M. Thorne, On the origin of plasmaspheric hiss: Ray path integrated amplification, *J. Geophys. Res.*, *88*, 7941, 1983.

Draganov, A. B., U. S. Inan, V. S. Sonwalkar, and T. F. Bell, Magnetospherically reflected whistlers as a source of plasmaspheric hiss, *Geophys. Res. Lett.*, *19*, 233, 1992.

Edgar, B. C., The upper and lower frequency cutoffs of magnetospherically reflected whistlers, *J. Geophys. Res.*, *81*, 205, 1976.

Green, J. L., D. A. Gurnett, and S. D. Shawhan, The angular distribution of auroral kilometric radiation, *J. Geophys. Res.*, *82*, 1825, 1977.

Kelley, M. C., K. D. Baker, J. C. Ulwick, C. L. Rino, and M. J. Baron, Simultaneous rocket probe, scintillation, and incoherent scatter observations of irregularities in the auroral zone ionosphere, *Radio Sci.*, *15*, 491, 1980.

Krall, N. A., and A. W. Trivelpiece, *Principles of Plasma Physics*, 674 pp., McGraw-Hill, New York, 1973.

Lefeuvre, F., M. Parrot, L. R. O. Storey, and R. R. Anderson, Wave distribution functions for plasmaspheric hiss observed on board ISEE 1, *Tech. Note LPCE/6*, Lab. de Phys. et chim. de l'Environ., Orleans, France, 1983.

Parrot, M., World map of ELF/VLF emissons as observed by a low-orbiting satellite, *Ann. Geophys.*, *8*, 135, 1990.

Shawhan, S. D., D. A. Gurnett, D. L. Odem, R. A. Helliwell, and C. G. Park, The Plasma Wave and Quasi-Static Electric Field Instrument (PWI) for Dynamics Explorer-A, in *Dynamics Explorer*, edited by R. A. Hoffman, p. 535, D. Reidel, Hingham, Mass., 1981.

Sonwalkar, V. S., T. F. Bell, R. A. Helliwell, and U. S. Inan, Direct multiple path magnetospheric propagation: a fundamental property of nonducted VLF waves, *J. Geophys. Res.*, *89*, 2823, 1984.

Sonwalkar, V. S., and U. S. Inan, Measurements of Siple transmitter signals on the DE 1 satellite: Wave normal direction and antenna effective length, *J. Geophys. Res.*, *91*, 154, 1986.

Sonwalkar, V. S., and U. S. Inan, Wave normal direction and spectral properties of whistler mode hiss observed on the DE 1 satellite, *J. Geophys. Res.*, *93*, 7493, 1988.

Sonwalkar, V. S., and U. S. Inan, Lightning as an embryonic source of VLF hiss, *J. Geophys. Res.*, *94*, 6986, 1989.

Storey, L. R. O., F. Lefeuvre, M. Parrot, L. Cairo, and R. R. Anderson, Initial survey of the wave distribution functions for plasmaspheric hiss, observed by ISEE 1, *J. Geophys. Res.*, *96*, 19,469, 1991.

Sulić, D. M., and G. Gustafsson, Study of Whistlers recorded by Viking, paper presented at XX General Assembly, Int. Union of Geod. and Geophys., Vienna, 1991.

Thorne, R. M., E. I. Smith, R. K. Burton, and R. E. Holzer, Plasmaspheric hiss, *J. Geophys. Res.*, *78*, 1581, 1973.

Uman, M. A. *The Lightning Discharge*, 377 pp., Academic, San Diego, Calif., 1987.

T. F. Bell, A. B. Draganov, U. S. Inan, and V. S. Sonwalkar, STAR Laboratory, Department of Electrical Engineering, Durand 324, Stanford University, Stanford, CA 94305.

(Received November 13, 1992;
revised February 25, 1993;
accepted March 9, 1993.)